The International Journal of Advanced Manufacturing Technology
https://doi.org/10.1007/s00170-024-14602-8

ORIGINAL ARTICLE

Experimental investigation of FDM manufacturing of 316 l stainless steel

Delia-Aurora Cerlincă[1] · Ioan Tamașag[1] · Irina Beșliu-Băncescu[1] · Traian-Lucian Severin[1] · Constantin Dulucheanu[1]

Received: 16 May 2024 / Accepted: 2 October 2024

Abstract

Continuous research in the field of metal additive manufacturing has led to the need for constant improvement of manufacturing parameters especially in the case of FDM (Fused Deposition Modeling) manufacturing. In recent years, the main directions outlined for productivity and quality improvement were related to higher printing speed and the use of ironing-type processes. This article aims to study the manufacturing parameters of the dimensional accuracy and surface quality of FDM-manufactured 316L stainless steel. The degree of novelty is given by the application of the ironing process for the green part. A full factorial 3^3 experimental design was designed for this study, in which the factors studied were ironing angle, ironing speed, and layer spacing during ironing. The dimensional accuracy and surface roughness were analyzed by means of deviation measurement from CAD to the green part and final part after the sintering process. Using the design of experiments offers the possibility of applying the analysis of variance (ANOVA) which provides information about the degree of influence of each of the studied factors. The results obtained for the dimensional accuracy showed that the ironing direction had the biggest influence on the Z-axis shrinkage. Overall, approximately 6% shrinkage in the Z and Y directions was obtained while in the X directions, the shrinkage percentage was around 20%. Surface roughness showed an improvement with higher ironing speeds for the green part while for the sintered part the most significant factor was ironing spacing.

Keywords Metal additive manufacturing · Metal FDM · Metal extrusion · Surface quality · 316L stainless steel

1 Introduction

The continuing development of additive manufacturing (AM) processes has led to the emergence of the possibility of additive manufacturing using various advanced ceramic [1] and metal-alloy [2] materials, including stainless steels [3, 4]. This is due to the many advantages of AM such as the fabrication of complex geometries in a relatively short time [5] and increased economics by reducing waste [6].

Recent studies [6, 7] have shown that the MEX (material extrusion [8]) process represents only 10% of all metal additive manufacturing methods, making more studies on this type of manufacturing necessary. One of the most studied materials used in Metal MEX is 316L stainless steel [6], used in various fields such as medical and military [9] due to its high mechanical-physical properties [6]. The manufacturing of metal parts by the MEX method involves the stepwise structure of additive manufacturing, from which the green part is obtained, debinding, from which the brown part is obtained and sintering from which the metal part is obtained [10]. Mainly, the debinding process involves removing the binder between the metal particles and sintering involves bonding them. Currently, there are 3 main types of debinding namely solvent debinding, catalytic debinding, and thermal debinding [11]. For catalytic debinding, the binder is changed from a solid state to a gaseous state by converting polyacetal binder to formaldehyde using nitric acid [11–14]. As for

✉ Ioan Tamașag
ioan.tamasag@usm.ro

Delia-Aurora Cerlincă
delia@usm.ro

Irina Beșliu-Băncescu
irina.besliu@usm.ro

Traian-Lucian Severin
severin.traian@usm.ro

Constantin Dulucheanu
dulu@usm.ro

[1] Faculty of Mechanical Engineering, Automotive and Robotics, "Ștefan cel Mare" University, 720229 Suceava, Romania

solvent debinding, a part of the binder is removed using chemical solvents such as acetone or ethanol [11], and the rest is removed in the sintering step [11, 13–16]. Thermal debinding involves placing the green part in a crucible together with refractory ballast and subjecting them to high temperatures using typical heat treatment furnaces [11, 13, 17–21].

Of the methods mentioned, thermal debinding can be considered the most cost-effective and environmentally friendly due to the fact that chemical solvents or nitric acid are no longer needed [11], an aspect that is attracting the attention of researchers and is being found in the literature in more and more studies. These include the aspect of dimensional accuracy and surface quality [11, 13–15, 22–28]. In terms of the debinding and sintering process, it has been found that better surfaces are obtained by reducing heating rates [23] and applying higher temperatures over longer periods of time [20]. Incomplete debinding can have a negative influence on the surfaces of the parts through the appearance of pores [15]. Other studies suggest that printing direction can influence dimensional accuracy [17], or even crucible dimensions can influence both dimensional accuracy and surface quality [11]. Regarding the manufacturing parameters, studies show that extrusion speed influences the porosity of 316L stainless steel MEX fabricated parts, while no trend was observed for the layer height variation [28]. In another research [26], the authors studied the influence of printing speed, layer height, and raster angle on the dimensional accuracy of additively manufactured 317L steel by the MEX method. The ANOVA analysis revealed that the significant factors were layer height and raster angle. Similarly, Quarto et al. [25] conducted a study in which they varied infill patterns, layer thickness, and extrusion speed and concluded that they have an impact on dimensional accuracy for AISI 316L additively fabricated by the MEX method. The results revealed that the optimum fabrication parameters were 0.1 mm for layer thickness and 20 mm/s for extrusion speed. The printing direction was studied by Tosto et al. [29], where the authors compared specimen sizes for both green parts and sintered parts for different printing directions. The results revealed that the upright printed parts showed higher anisotropic behavior compared with the flatwise specimens.

Although there are a number of studies in the literature, more research is needed on manufacturing parameters, especially as new manufacturing processes and parameters such as manufacturing speeds above 300 mm/s and the application of ironing are emerging. Also, many of the research articles were made using different manufacturers for the filament, usually BASF Ultrafuse 316L, which cannot be compared with other manufacturers. Regarding the ironing process, several studies have been conducted [30–33], but for the case of Metal MEX, the literature provides limited information; hence, the opportunity for research and novelty arises.

The aim and the degree of novelty of the article are given by the study of surface roughness and dimensional accuracy of 316L parts additively manufactured by the MEX method, using a full factorial design in which the varied factors are ironing angle, ironing speed, and ironing spacing. Normally, in additive manufacturing, these factors directly influence the surface quality and mechanical properties of the resulting parts [34, 35], but as yet, there are no studies on their influence in the case of MEX metallic additive manufacturing. Surface roughness and dimensional accuracy were considered for both green parts and sintered parts. Moreover, optical analysis of the surfaces before and after the sintering process was followed. In order to achieve the proposed objectives, a full factorial experimental design of type 3^3 was used, from which ANOVA analysis can be applied, indicating the degree of influence of the studied factors and the creation of variation graphs of the mean effects. In order to eliminate errors due to the debinding and sintering process, a single piece with 27 surfaces was made.

The results obtained from this study can contribute to the scientific community studying additive manufacturing of the MEX type, by applying a series of researches that can implicitly lead to the improvement of the metal additive manufacturing process and closer to the possibility of replacing the classic manufacturing process.

2 Materials and methods

2.1 Establishing the experimental design

The proposed factorial design is shown in Table 1, with values for levels and parameters in Table 2. The experimental design is based on a full factorial design of the DOE 3^3 type with 27 experiments, which allows the systematic study either individually or in combination with the main effects of the studied input factors. After the testing parts manufacturing and measuring, an ANOVA analysis was used to quantify the significance of each factor and their interactions with the response variables.

The values chosen for the input factor levels were selected to capture a range of conditions that are practical and relevant to the ironing process. The directions represent orientations that could significantly impact surface finish and dimensional accuracy, with 0° being aligned with the build direction, 90° perpendicular to the build direction, and 45° as a midpoint. The ironing speeds of 10, 20, and 30 mm/s cover a range of slow to fast passes, providing insight into the effect of speed on heat generation and surface smoothing. Similarly, the chosen spacing values (0.1, 0.2, and 0.3 mm) represent progressively larger gaps between ironing passes,

Table 1 L27 complete DOE design

Nr	Ironing angle [°]	Ironing speed [mm/s]	Ironing spacing [mm]
1	1	1	1
2	1	1	2
3	1	1	3
4	1	2	1
5	1	2	2
6	1	2	3
7	1	3	1
8	1	3	2
9	1	3	3
10	2	1	1
11	2	1	2
12	2	1	3
13	2	2	1
14	2	2	2
15	2	2	3
16	2	3	1
17	2	3	2
18	2	3	3
19	3	1	1
20	3	1	2
21	3	1	3
22	3	2	1
23	3	2	2
24	3	2	3
25	3	3	1
26	3	3	2
27	3	3	3

Table 2 Factors levels and values

Level	Ironing angle [°]	Ironing speed [mm/s]	Ironing spacing [mm]
1	0	10	0.1
2	45	20	0.2
3	90	30	0.3

allowing for an investigation of the impact on material flow and surface uniformity.

2.2 Test specimen manufacturing

The filament used for these studies (marketed by The Virtual Foundry, USA) is composed of 85.8% 316L stainless steel, with the remainder up to 100% polylactic acid (PLA) binder [36, 37]. The chemical composition of the filament, according to the datasheet, is shown in Table 3. The exact composition values and binding additive name and percentage information are omitted as it is a trade secret.

Table 3 Used filament chemical composition [37]

Material	Iron	Nickel	Chromium	Molybdenum	Polylactic acid
% by weight	40.00–63.75	4.00–17.00	4.00–17.00	0.80–4.25	< 20%

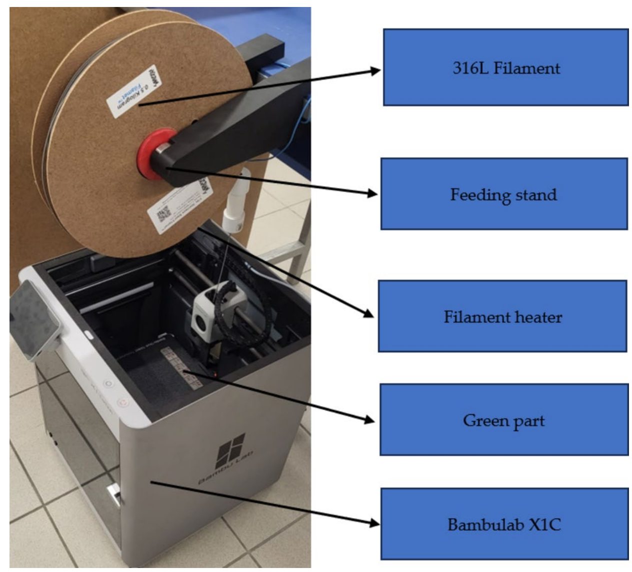

Fig. 1 Additive manufacturing setup

The actual manufacturing of the green stage specimens was done using a Bambulab X1Carbon FDM (Fused Deposition Modeling) printer. Due to the ductile nature of the filament, for ease of fabrication, a filament warmer (Filawarmer offered by the same company that produces the filament) was used to keep the filament at a constant temperature of 60 °C, soften the material, and thus facilitate its feeding into the extruder of the printer (Fig. 1). To simplify the fabrication process, a filament roll holder was made and positioned above the printer, allowing the filament to be fed directly into the extruder without bending it and risking breakage.

Constant additive manufacturing parameters correspond to Table 4. Due to the abrasive nature of the filament and to avoid nozzle clogging during the manufacturing process, a heat-treated steel nozzle with a diameter of 0.8 mm was used.

The shape of the specimens according to the levels in the full factorial plane corresponds to Fig. 2, where the direction, speed, and spacing of the ironing process can be seen. Due to the fact that sintering temperature and duration can influence the studied output parameters, a single piece with 27 test areas was considered in which the presented factors

Table 4 Constant manufacturing parameters

Parameter	Value	Parameter	Value
Layer height	0.4 mm	Retraction	6.5 mm
Nozzle temperature	220°	Wall number	1
Printing speed	100 mm/s	Infill	70%
Build platform temperature	35°	Nozzle size	0.8 mm

were varied. Figure 2a shows the specimens in the slicer software (BambuStudio, version 1.9.2.57). Within the test specimen, a non-ironed surface was also included in order to compare the results.

2.3 Specimen sintering

For the debinding and sintering process, a Carbolite-type furnace with temperature adjustment up to 1600 °C was used (Fig. 3a). The FDM specimen was placed in a crucible with the dimensions shown in Fig. 3b, where the filament manufacturers' recommendations for the positioning of the part were maintained. To ensure the stability of the part during the debinding and sintering process, a mixture of Al203 and graphite was used as sintering powder.

The debinding and sintering process was carried out according to the specifications provided by the filament manufacturer. The parameters used in this process are shown in Table 5, which explains Fig. 4.

2.4 Measurement and optical analysis of specimens

Normally, following the sintering process, the resulting parts show dimensional variations due to the shrinkage effect, which must be taken into account in the part design stage [38]. Dimensional deviations were measured using a Mahr 40 EX micrometer and a Mahr 16 EX caliper for both the green and sintered specimens. In order to provide a high degree of confidence in the experimental studies, the

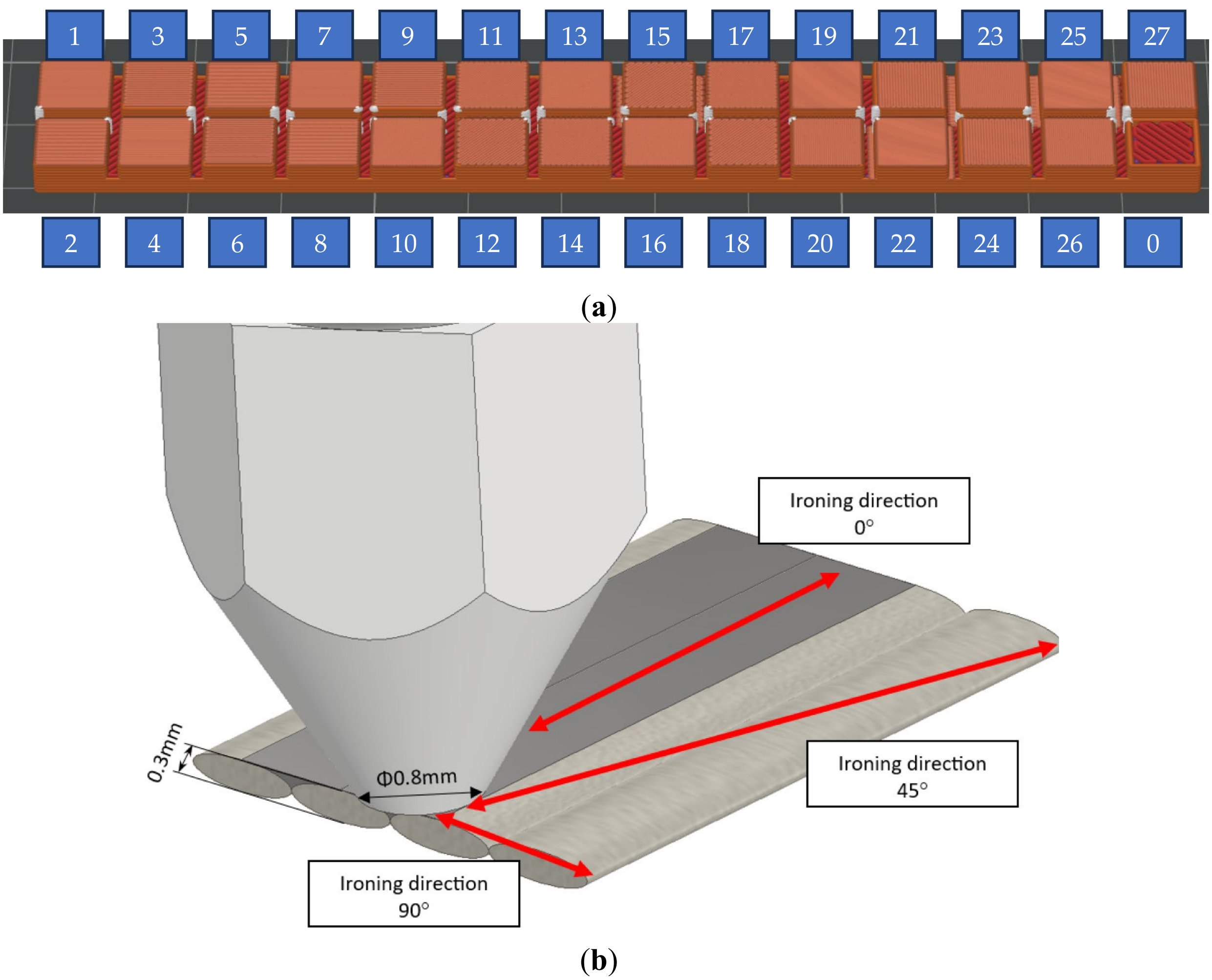

Fig. 2 Varied manufacturing parameters: **a** slicer view; **b** ironing exemplification

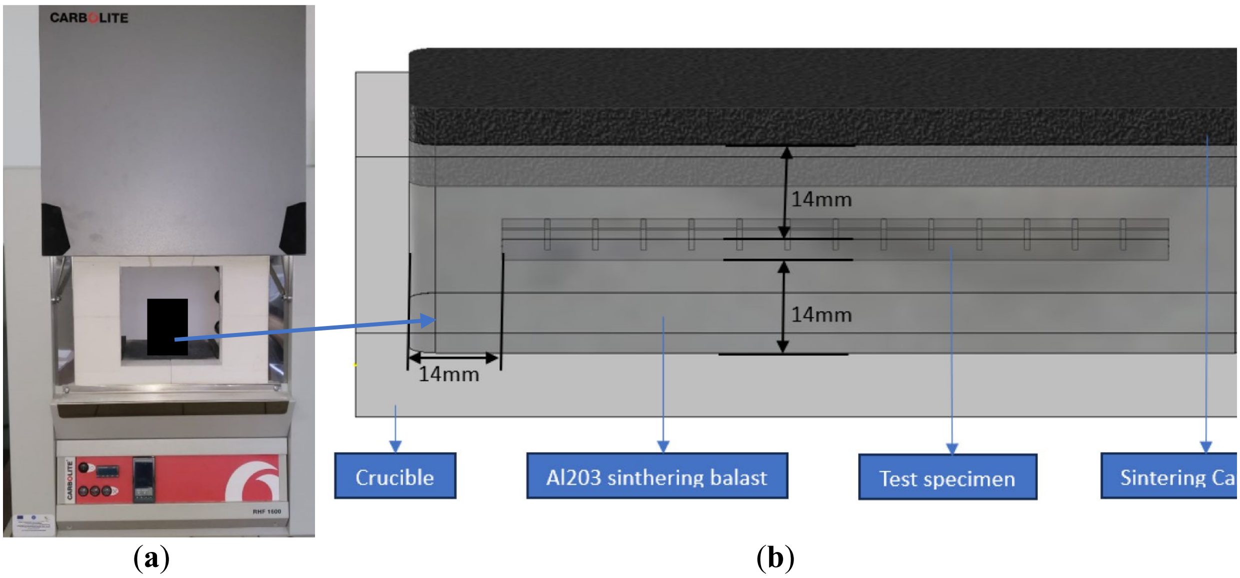

Fig. 3 Debinding and sintering equipment: **a** kiln; **b** crucible

Table 5 Debinding and sintering steps

Debinding	Time	Temperature	Sintering	Time	Temperature
Ramp	2 h	204 °C	Ramp	Fastest possible	593 °C
Hold	2 h	204 °C	Hold	2 h	593 °C
Ramp	2 h	407 °C	Ramp	2 h	1287 °C
Hold	2 h	407 °C	Hold	4 h	1287 °C
Cooldown	Normal cooldown		Ramp	6 h	593 °C
			Cooldown	Normal cooldown	

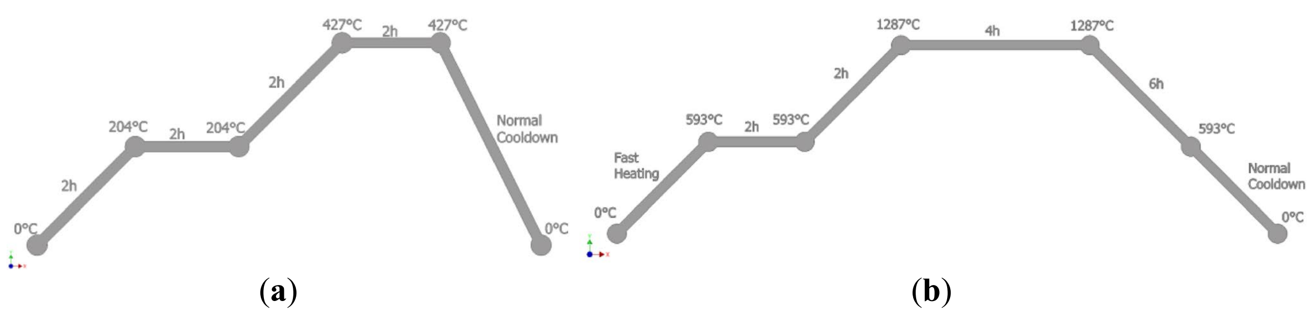

Fig. 4 Schematic debinding and sintering process: **a** debinding; **b** sintering

specimen dimensions were compared with others found in the literature. The measurements of the specimens were carried out for each individual area to determine the variations in the factors studied as well as the deviations on the other two axes (X and Y) (Fig. 5).

Subsequently, the surfaces were analyzed for roughness using a Mahr CWM100 confocal microscope, from which 3D images of the measured surfaces were taken (Fig. 6).

For optical analysis, images of the surfaces were taken using an Optech" microscope model IM/IMT (manufacturer: Exacta + Optech GmbH, Munich, Germany). Subsequently, the dedicated microscopic analysis software ImageJ 1.54G was used, provided by Wayne Rasband and contributors, National Institute of Health, USA, after the calibration the crater areas (pores) obtained during the sintering process were measured (Fig. 7).

Fig. 5 Deviation measurement: **a** equipment; **b** green and sintered part

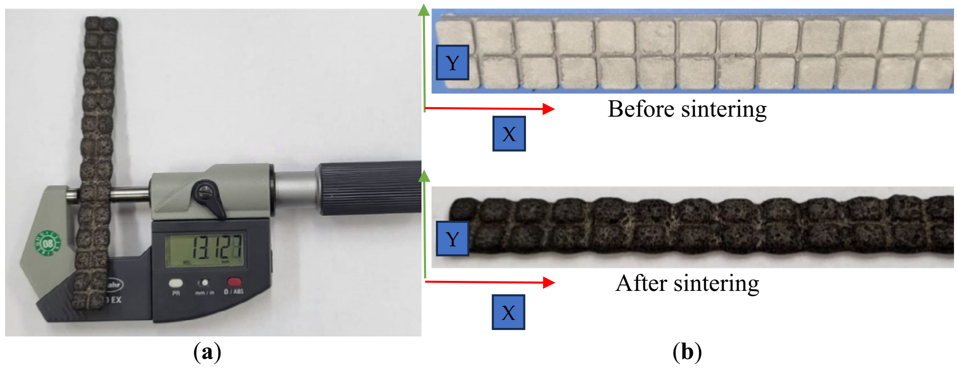

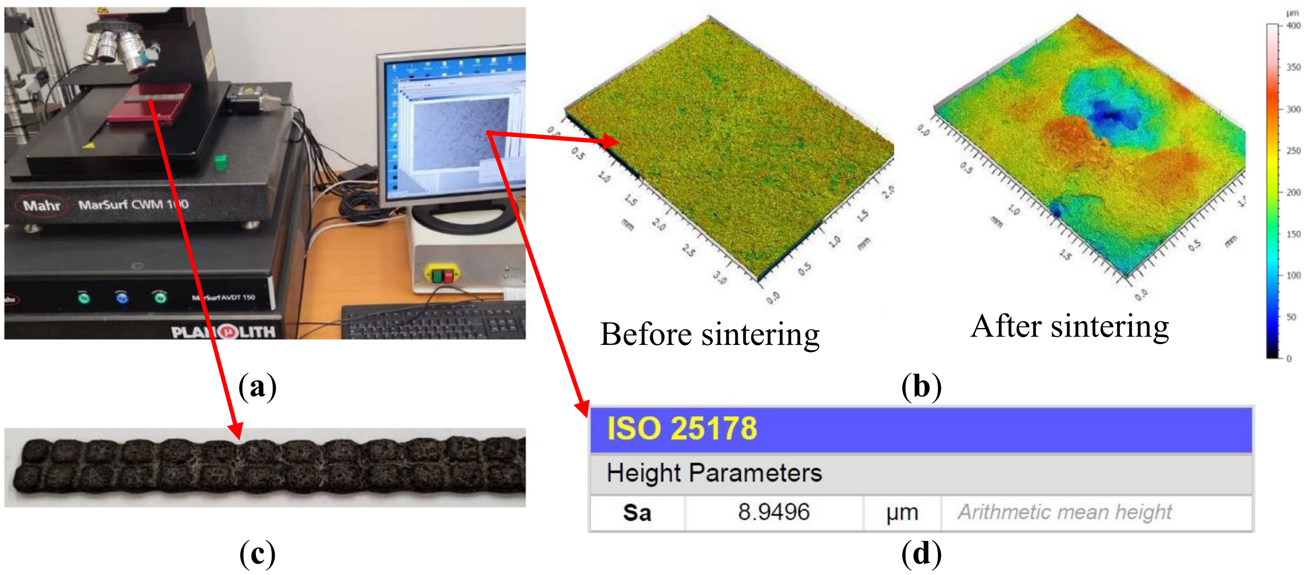

Fig. 6 Surface roughness measurement: **a** equipment; **b** obtained images; **c** green and sintered part; **d** obtained results

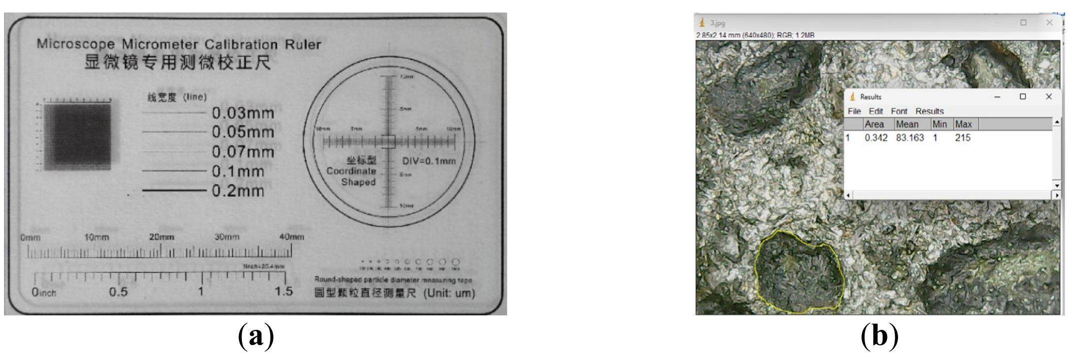

Fig. 7 Pore measurement: **a** calibration ruler, **b** ImageJ analysis

3 Results and discussions

The experimental results obtained have been entered in Table 6.. Using Minitab statistical analysis software, it was possible to plot the mean effect variances and apply ANOVA analysis to determine statistically significant factors (p-value < 0.5).

Table 6. Obtained results

Exp	Ironing angle [°]	Ironing speed [mm/s]	Ironing spacing [mm]	Green part, Sa [µm]	Sintered part, Sa [µm]	Green part, h [mm]	Sintered part, h [mm]
1	1	1	1	8.123	92.048	4.085	3.775
2	1	1	2	15.80	55.150	4.180	3.896
3	1	1	3	11.26	23.882	4.125	3.865
4	1	2	1	12.60	35.073	4.225	3.975
5	1	2	2	7.966	21.859	4.163	3.753
6	1	2	3	10.12	31.503	4.216	3.908
7	1	3	1	18.32	26.356	4.074	3.743
8	1	3	2	9.110	25.986	4.145	3.727
9	1	3	3	10.18	58.469	4.120	3.717
10	2	1	1	22.26	55.245	4.095	3.512
11	2	1	2	10.56	57.002	4.049	3.675
12	2	1	3	10.15	21.235	4.065	3.474
13	2	2	1	7.490	37.151	4.062	3.701
14	2	2	2	13.62	45.466	4.052	3.580
15	2	2	3	12.99	50.884	4.077	3.625
16	2	3	1	6.290	32.571	4.042	3.539
17	2	3	2	8.840	22.649	4.066	3.601
18	2	3	3	8.949	37.284	4.050	3.665
19	3	1	1	9.398	30.443	4.029	3.507
20	3	1	2	7.826	23.769	4.021	3.509
21	3	1	3	10.46	25.692	4.022	3.465
22	3	2	1	8.794	19.418	4.020	3.530
23	3	2	2	9.316	35.111	4.023	3.724
24	3	2	3	10.19	29.585	4.020	3.680
25	3	3	1	7.624	26.921	4.024	3.355
26	3	3	2	10.28	26.774	4.031	3.713
27	3	3	3	7.197	29.117	4.092	3.818

3.1 Dimensional accuracy

In the first phase, green stage measurements of the specimens were carried out, and the results allowed the plotting of the variation of the mean effects shown in Fig. 8.

According to the results, it can be seen that the direction of ironing influences the dimensions of the part. There was a decrease of 2.08% when changing the direction from 0 to 45°, followed by a decrease of 0.75% from 45 to 90°. This may be due to the fact that when ironing at an angle other than 0°, the printing direction is no longer parallel to the printing direction of the previous layer, resulting in a leveling effect by squeezing the asperities. As for the ironing speed, an insignificant parabolic variation can be observed with a total variation of 0.08% between the speed of 10 and 30 mm/s. For the case of the distance between crossings, a linear increasing trend can be observed by increasing the spacing dimensions. As in the case of the ironing angle, this may be due to the squeezing effect.

ANOVA analysis allowed the determination of statistically significant factors (p-value < 0.05), from which the graph in Fig. 9 was obtained. It can be seen that the statistically significant factor is the ironing angle, with a significance percentage of 86.71%, followed by the other non-significant factors, namely spacing with 10.98% and ironing speed with 2.31%.

After analyzing the results for green specimens, the analysis was carried out for sintered specimens. According to the graphs (Figs. 10 and 11), it can be seen that the trends are similar to the previous case. There was a decrease of 5.78% from 0 to 45° followed by a decrease of 0.22% between 45 and 90°, the ironing speed shows a parabolic trend, and the spacing shows an increasing trend. The measured values for green parts are given in Table 7 and for sintered parts in Table 8.

As with the green parts, the statistically significant factor is the ironing angle with an influence of 75.52%, followed by spacing with 20.44% and print speed with 7.05%.

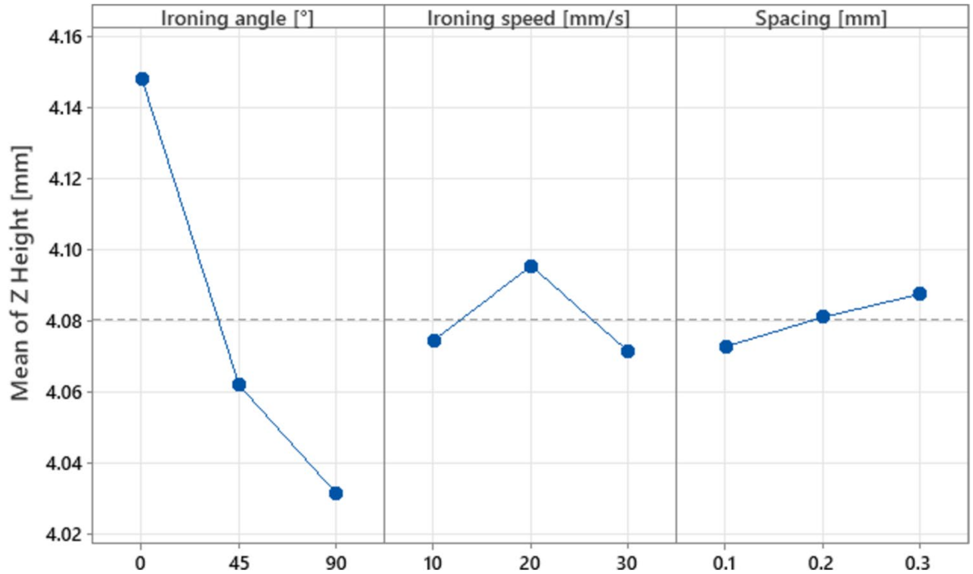

Fig. 8 Variation graph for the green part

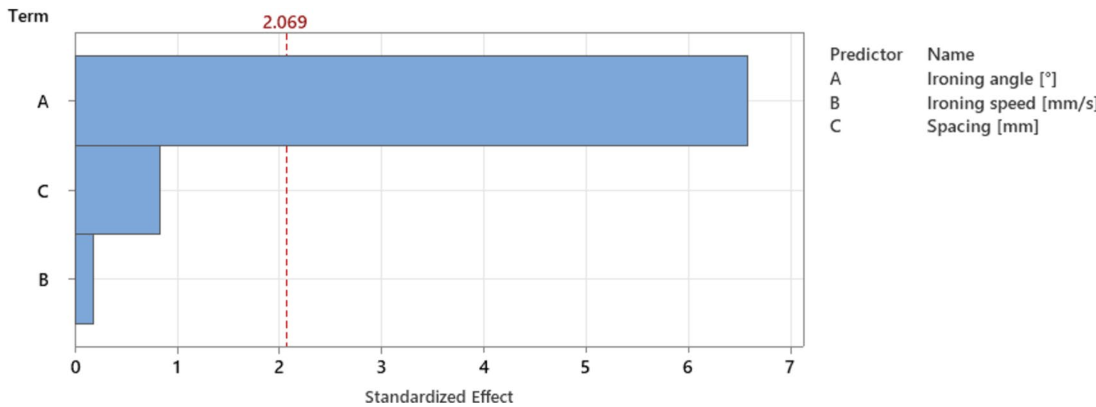

Fig. 9 Pareto chart for Z height of the green part

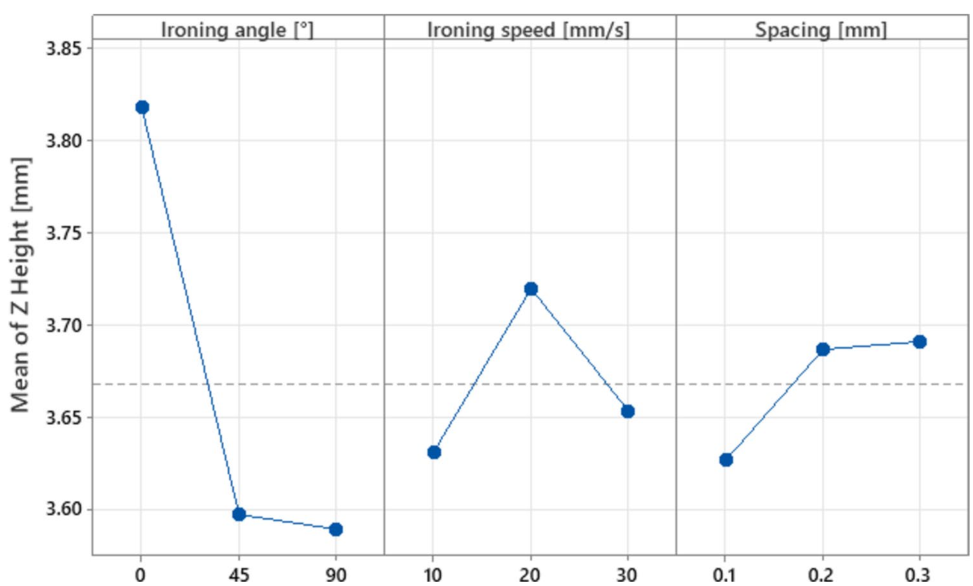

Fig. 10 Variation graph for the sintered part

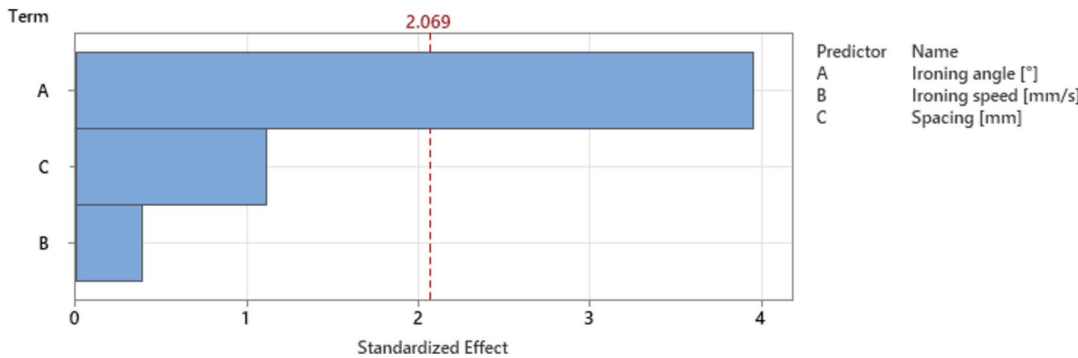

Fig. 11 Pareto chart for Z height of the sintered part

Table 7 Main effect variations for Z height before sintering

	Level	Ironing angle [°]		Ironing speed [mm/s]		Spacing [mm]	
		Value	Variation	Value	Variation	Value	Variation
Before sintering	1	0	-	10	-	0.1	-
	2	45	↓ 2.08%	20	↓ 0.51%	0.2	↑ 0.2%
	3	90	↓ 0.75%	30	↓ 0.59%	0.3	↑ 0.17%
Total variation		From 0 to 90	↓ 2.81%	From 10 to 30	↓ 0.08%	From 0.1 to 0.3	↑ 0.36%

Table 8 Main effect variations for Z height after sintering

	Level	Ironing angle [°]		Ironing speed [mm/s]		Spacing [mm]	
		Value	Variation	Value	Variation	Value	Variation
After sintering	1	0	-	10	-	0.1	-
	2	45	↓ 5.78%	20	↑ 2.44%	0.2	↑ 1.66%
	3	90	↓ 0.22%	30	↓ 1.79%	0.3	↑ 0.12%
Total variation		From 0 to 90	↓ 5.99%	From 10 to 30	↑ 0.61%	From 0.1 to 0.3	↑ 1.78%

Table 9 Main effect variations for Z height after sintering

Part	Mean value X direction [mm]	Mean value Y direction [mm]	Mean value Z direction [mm]
Green	16.98	125.01	4.08
Sintered	13.62	118.38	3.67
Shrinkage	19.79%	5.59%	10.05%

The total average deviations between the green part and the sintered part have been entered in Table 9. There was a deviation of 19.79% on the X-axis, 5.59% on the Y-axis, and 10.05% on the Z-axis.

The values for the Y- and Z-axis deviations are consistent with the trends obtained by researchers in the literature [29]. However, for the X-axis, a shrinkage of about 20% was recorded. This may be due to heat flow. Considering that the workpiece was positioned in the furnace according to Fig. 12, it can be considered that the heat flow first enters with a direction perpendicular to the X-axis of the workpiece undergoing sintering, mainly due to the fact that the crucible geometry is rectangular, thus making the heat transferal not uniform.

3.2 Optical analysis

Both the optical analysis using the confocal microscope and the Optika microscope showed that for the case of green parts, all studied factors have an influence. Figure 13 shows images of surfaces in different manufacturing conditions according to the experimental design. It can be seen that by increasing the values of ironing angle, speed, and spacing, the metal particles are evenly distributed and the resulting surfaces are smoother. In the case of using ironing at low speeds, clusters of material can be observed gathered in the printing direction. However, a substantial improvement is observed for all cases where ironing has been applied compared to the case of the surface where no ironing has been applied, where traces of layer thickness and clusters of metal particles are observed.

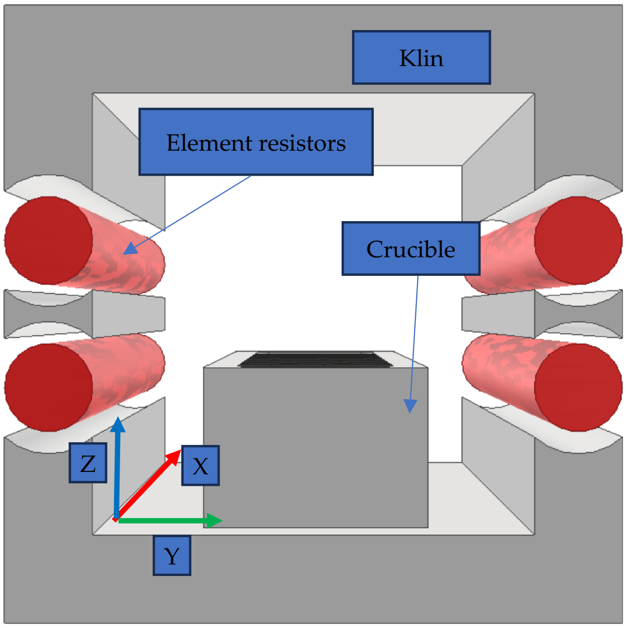

Fig. 12 Heat flux direction on the crucible

These aspects can also be observed for sintered surfaces. Figure 14 shows the surfaces studied after sintering. It can be seen that by increasing any of the studied factors (ironing angle, speed, and spacing), the surfaces show different structures. The analysis of the images using the dedicated ImageJ software revealed that at low values, the surfaces show larger pore sizes, and as the values of the factors increase, the pores observed are of smaller sizes but appear more often. These aspects can confirm the formation of clusters at low values of velocity and spacing but also the occurrence of the smoothing effect, whereby changing the ironing angle, the ironing direction is no longer parallel to the printing direction of the previous layer, and therefore, the distribution of metal particles is no longer linear.

The variation of the recorded values for the surface areas of the created pores falls within the range 0.615–0.012 mm^2.

3.3 Surface roughness

The optical analysis performed is also consistent with the values obtained for surface roughness. For the case of green surfaces, decreasing trends were observed for all factors studied. The percentage variations have been entered in Table 10. For the ironing angle, a decreasing trend can be observed, similar to the case of dimensional deviations presented in Sect. 3.1 and Fig. 15. A total decrease of 21.63% was obtained when varying the ironing angle between 0 and 90°. As in the previous case, this may be due to the roughening effect or uniform distribution of the metal particles.

In terms of ironing speed, there was a decrease of 12.04% when using 20 mm/s speed compared to 10 mm/s speed and a decrease of 6.77% when using 30 mm/s speed compared to 20 mm/s speed, registering a total decrease of 18.00% between 10 and 30 mm/s. This may be due to the deposition velocity of the metal particles, which influences cluster formation.

Fig. 13 Green parts optical images

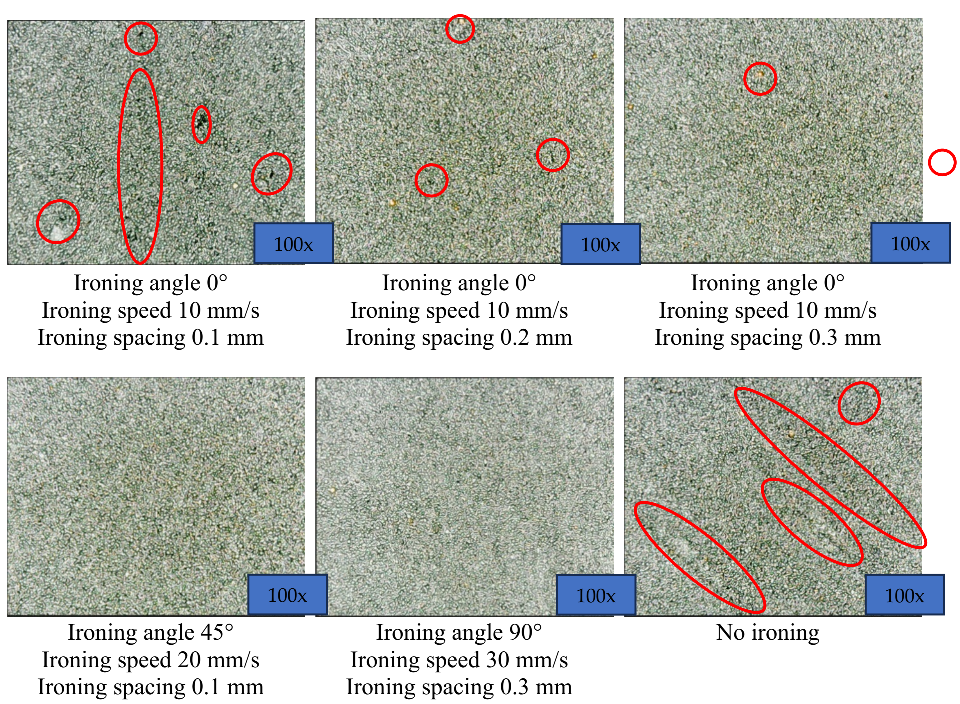

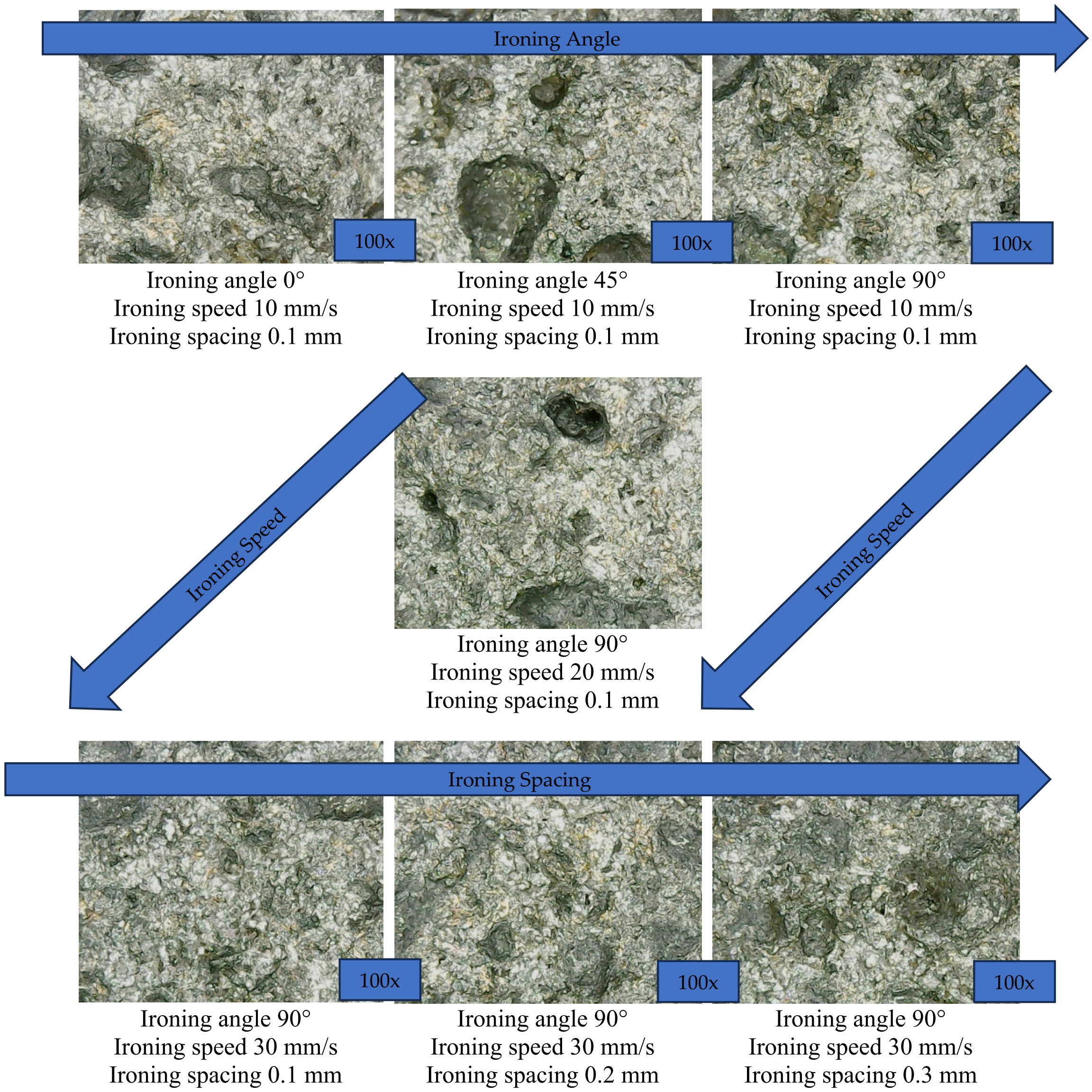

Fig. 14 Parts optical images after sintering

Table 10 Main effect variations for Sa before sintering

	Level	Ironing angle [°]		Ironing speed [mm/s]		Spacing [mm]	
		Value	Variation	Value	Variation	Value	Variation
Before sintering	1	0	-	10	-	0.1	-
	2	45	↓ 2.24%	20	↓ 12.04%	0.2	↓ 7.51%
	3	90	↓ 19.84%	30	↓ 6.770%	0.3	↓ 1.95%
Total variation		From 0 to 90	↓ 21.63%	From 10 to 30	↓ 18.00%	From 0.1 to 0.3	↓ 9.31%

For the spacing case, there was a total decrease of 9.31% between the first value used in the experimental design and the last one.

The ANOVA analysis allowed the Pareto chart in Fig. 16 to be plotted, from which it can be seen that none of the factors is statistically significant. However, there was a significance of 44.04% for ironing angle, 37. 48% for ironing speed, and 18. 48% for ironing spacing.

As with green parts, roughness values show approximately the same trends for sintered surfaces (Fig. 17). There was a decrease of 2.93% when varying the ironing angle from 0 to 45° followed by a sharp decrease of 31.34%

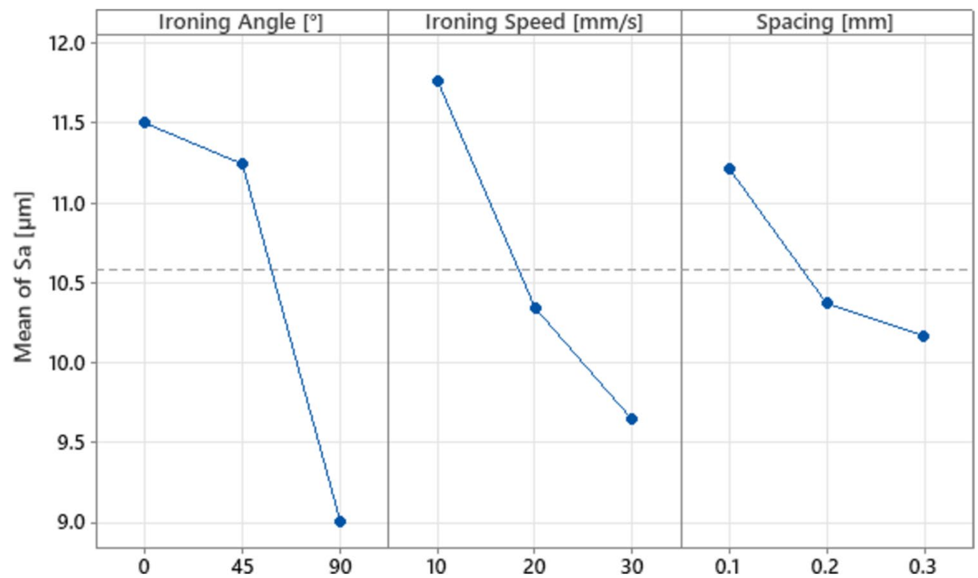

Fig. 15 Main effect variation graph for Sa of the green part

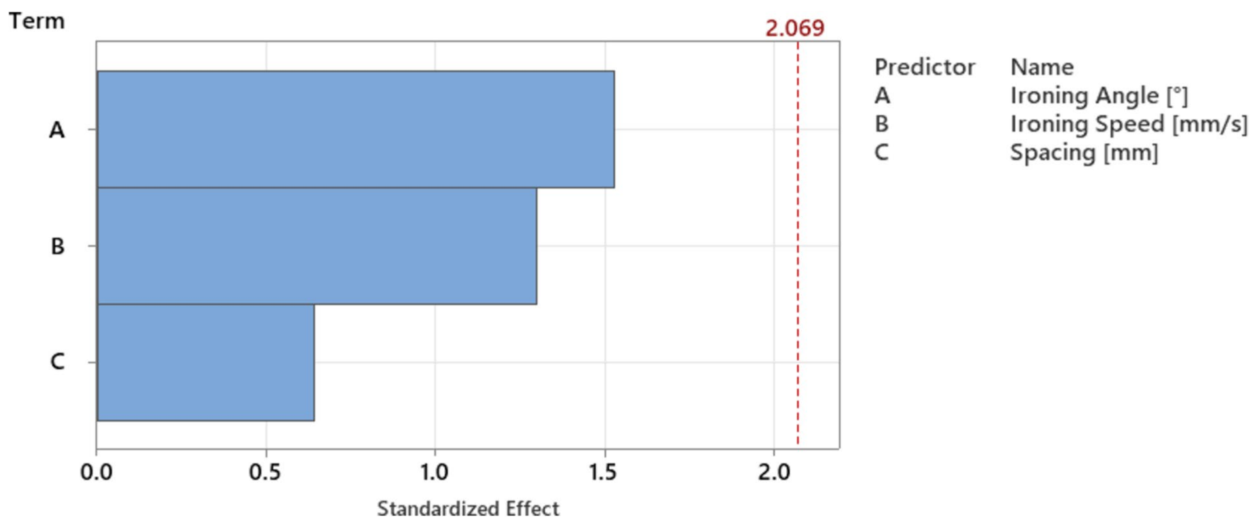

Fig. 16 Pareto chart for Sa of the green part

when varying the ironing angle from 45 to 90°, giving a total of 33.35% improvement in surface roughness. For ironing speed, a total variation of 25.58% was obtained, and for spacing, a variation of 13.39%. These values have been entered in Table 11.

The ANOVA analysis gave values close to the case of green-stage parts. The Pareto plot in Fig. 18 shows that no factor is statistically significant. There was a significance of 45.04% for ironing angle, 36.5% for ironing speed, and 17.66% for ironing spacing.

4 Conclusions

The presented study investigated the influence of ironing parameters (ironing angle, ironing speed, and ironing spacing) on surface quality and dimensional accuracy in additive manufacturing of 316L stainless steel. The results indicate a number of significant effects of these parameters on the final properties of the manufactured part, providing valuable insights for optimizing production processes.

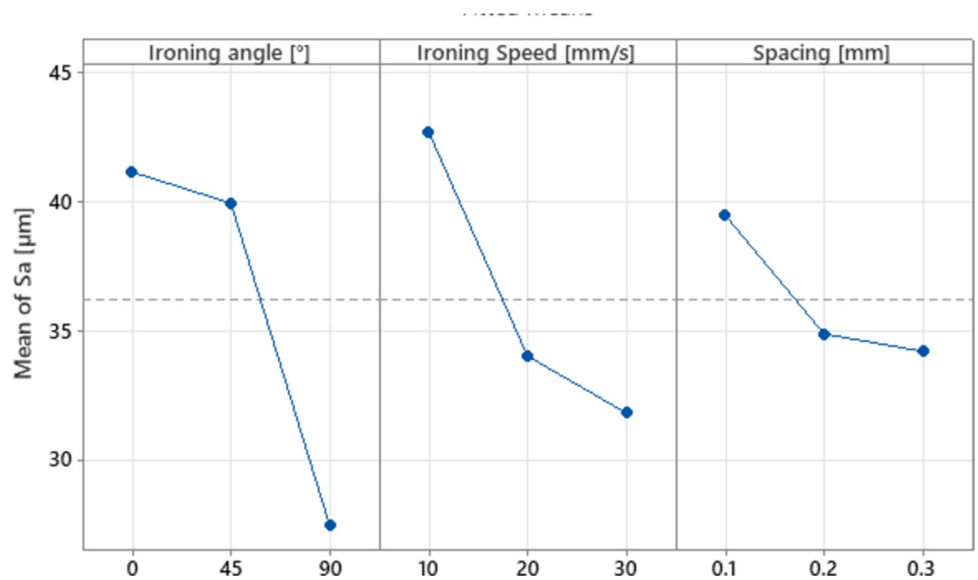

Fig. 17 Main effect variation graph for Sa of the parts after sintering

Table 11 Main effect variations for Sa after sintering

	Level	Ironing angle [°]		Ironing speed [mm/s]		Spacing [mm]	
		Value	Variation	Value	Variation	Value	Variation
After sintering	1	0	-	10	-	0.1	-
	2	45	↓ 2.930%	20	↓ 20.4%	0.2	↓ 11.67%
	3	90	↓ 31.34%	30	↓ 6.51%	0.3	↓ 1.950%
Total variation		From 0 to 90	↓ 33.35%	From 10 to 30	↓ 25.58%	From 0.1 to 0.3	↓ 13.39%

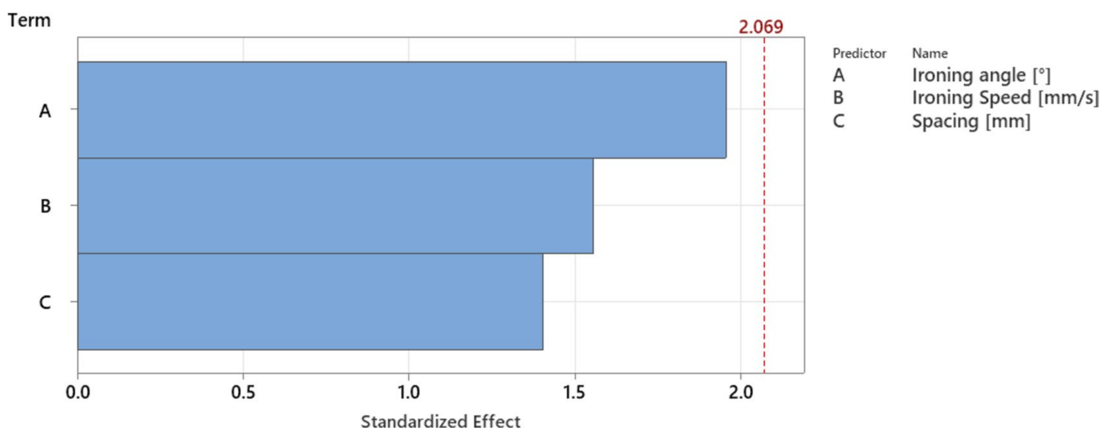

Fig. 18 Pareto chart for Sa of the green part

The first major observation is that increasing the ironing speed reduces the roughness of the surface. This effect can be attributed to the fact that a higher speed minimizes the exposure time of the material to the heat generated during the ironing process, thus reducing the opportunity for the formation of microstructural defects that can increase roughness. In contrast, ironing speed did not have a significant impact on dimensional accuracy, suggesting that this parameter can be adjusted to improve surface finish without compromising the structural dimensions of the part in both the green and sintered stages. An overall roughness improvement of 25.58% was recorded between the ironing speed of 10 mm/s and 30 mm/s for sintered parts.

Increasing the ironing angle changed the printing direction, making it easier to pass perpendicularly over the previous layers. This led to the flattening of the roughness and a leveling effect, which also facilitated the dimensional accuracy of the parts in the green stage. This improved layer orientation can be used to control the anisotropy of mechanical properties, which is a common challenge in additive manufacturing. For the case of sintered surfaces, improvements of up to 33.35% were observed when ironing angles other than 0° (which represents ironing parallel to the last deposited layer) were used.

Another important finding is that by increasing the ironing gap, the initial dimensions of the part before sintering were increased, and the surface quality improved by eliminating the formation of large pores. It appears that a larger space allows better heat distribution and reduces particle agglomeration, factors that contribute to more uniform densification and reduced surface defects.

It was observed that by increasing all the factors studied, the green piece showed reduced surface defects, which implicitly led to reduced sintered surface defects. In principle, sintered surfaces showed smaller pore sizes when ironing parameters with higher values were used.

In conclusion, the application of the ironing process and the optimization of ironing angle, ironing speed, and ironing spacing present an effective method for improving quality and accuracy in additive manufacturing of 316L stainless steel. However, they do not eliminate the need for finishing by classical surface chipping processes. In view of these issues, more studies are needed to better understand the effect of ironing in MEX fabrication.

Author contribution All authors contributed to the study's conception and design. Material preparation, data collection, and analysis were performed by Delia-Aurora Cerlincă, Ioan Tamașag, Irina Beșliu-Băncescu, Traian-Lucian Severin, and Constantin Dulucheanu. The first draft of the manuscript was written by Delia-Aurora Cerlincă and Ioan Tamașag, and all authors commented on previous versions of the manuscript. All authors read and approved the final manuscript.

Data availability Not applicable.

Declarations

Consent to participate Not applicable.

Consent for publication Not applicable.

Conflict of interest The authors declare no competing interests.

References

1. Chen Z, Li Z, Li J, Liu C, Lao C, Fu Y, Liu C, Li Y, Wang P, He Y (2019) 3D Printing of ceramics: a review. J Eur Ceram Soc 39:661–687. https://doi.org/10.1016/j.jeurceramsoc.2018.11.013
2. Singh P, Balla VK, Tofangchi A, Atre SV, Kate KH (2020) Printability studies of Ti-6Al-4V by metal fused filament fabrication (MF3). Int J Refract Metal Hard Mater 91:105249. https://doi.org/10.1016/j.ijrmhm.2020.105249
3. Kurose T, Abe Y, Santos MVA, Kanaya Y, Ishigami A, Tanaka S, Ito H (2020) Influence of the layer directions on the properties of 316L stainless steel parts fabricated through fused deposition of metals. Materials 13:2493. https://doi.org/10.3390/ma13112493
4. Godec D, Cano S, Holzer C, Gonzalez-Gutierrez J (2020) Optimization of the 3D printing parameters for tensile properties of specimens produced by fused filament fabrication of 17–4PH stainless steel. Materials 13:774. https://doi.org/10.3390/ma13030774
5. Shirazi SFS, Gharehkhani S, Mehrali M, Yarmand H, Metselaar HSC, Adib Kadri N, Osman NAA (2015) A review on powder-based additive manufacturing for tissue engineering: selective laser sintering and inkjet 3D printing. Sci Technol Adv Mater 16:033502. https://doi.org/10.1088/1468-6996/16/3/033502
6. Ramazani H, Kami A (2022) Metal FDM, a new extrusion-based additive manufacturing technology for manufacturing of metallic parts: a review. Prog Addit Manuf 7:609–626. https://doi.org/10.1007/s40964-021-00250-x
7. Vafadar A, Guzzomi F, Rassau A, Hayward K (2021) Advances in metal additive manufacturing: a review of common processes, industrial applications, and current challenges. Appl Sci 11:1213. https://doi.org/10.3390/app11031213
8. ISO/ASTM 52900 (2021) International Standard: 2021 Additive manufacturing—general principles—fundamentals and vocabulary. ISO/ASTM International: Geneva, Switzerland
9. Weston NS, Thomas B, Jackson M (2019) Processing metal powders via field assisted sintering technology (FAST): a critical review. Mater Sci Technol 35:1306–1328. https://doi.org/10.1080/02670836.2019.1620538
10. Liu B, Wang Y, Lin Z, Zhang T (2020) Creating metal parts by fused deposition modeling and sintering. Mater Lett 263:127252. https://doi.org/10.1016/j.matlet.2019.127252
11. Wei X, Li X, Bähr R (2024) Optimizing metal part distortion in the material extrusion-thermal debinding-sintering process: an experimental and numerical study. Heliyon 10:e28899. https://doi.org/10.1016/j.heliyon.2024.e28899
12. Rosnitschek T, Glamsch J, Lange C, Alber-Laukant B, Rieg F (2021) An automated open-source approach for debinding simulation in metal extrusion additive manufacturing. Designs 5:2. https://doi.org/10.3390/designs5010002
13. Agne A, Barrière T (2017) Modelling and numerical simulation of supercritical CO2 debinding of Inconel 718 components elaborated by metal injection molding. Appl Sci 7:1024. https://doi.org/10.3390/app7101024
14. Sadaf M, Bragaglia M, Nanni F (2021) A simple route for additive manufacturing of 316L stainless steel via fused filament fabrication. J Manuf Process 67:141–150. https://doi.org/10.1016/j.jmapro.2021.04.055

15. Gonzalez-Gutierrez J, Cano S, Schuschnigg S, Kukla C, Sapkota J, Holzer C (2018) Additive manufacturing of metallic and ceramic components by the material extrusion of highly-filled polymers: a review and future perspectives. Materials 11:840. https://doi.org/10.3390/ma11050840
16. Singh G, Missiaen J-M, Bouvard D, Chaix J-M (2021) Copper additive manufacturing using MIM feedstock: adjustment of printing, debinding, and sintering parameters for processing dense and defectless parts. Int J Adv Manuf Technol 115:449–462. https://doi.org/10.1007/s00170-021-07188-y
17. Wei X, Behm I, Winkler T, Scharf S, Li X, Bähr R (2022) Experimental study on metal parts under variable 3D printing and sintering orientations using bronze/PLA hybrid filament coupled with fused filament fabrication. Materials 15:5333. https://doi.org/10.3390/ma15155333
18. Amin AM, Ibrahim MHI, Asmawi R, Mustaffa N, Hashim MY (2017) Thermal debinding and sintering of water atomised SS316L metal injection moulding process. IOP Conf Ser: Mater Sci Eng 226:012155. https://doi.org/10.1088/1757-899X/226/1/012155
19. Hwang KS, Tsou TH (1992) Thermal debinding of powder injection molded parts: observations and mechanisms. Metall Trans A 23:2775–2782. https://doi.org/10.1007/BF02651756
20. Supriadi S, Suharno B, Hidayatullah R, Maulana G, Baek ER (2017) Thermal debinding process of SS 17–4 PH in metal injection molding process with variation of heating rates, temperatures, and holding times. SSP 266:238–244. https://doi.org/10.4028/www.scientific.net/SSP.266.238
21. Mousapour M, Salmi M, Klemettinen L, Partanen J (2021) Feasibility study of producing multi-metal parts by fused filament fabrication (FFF) technique. J Manuf Process 67:438–446. https://doi.org/10.1016/j.jmapro.2021.05.021
22. Enneti RK, Park SJ, German RM, Atre SV (2012) Review: thermal debinding process in particulate materials processing. Mater Manuf Process 27:103–118. https://doi.org/10.1080/10426914.2011.560233
23. Thompson Y, Gonzalez-Gutierrez J, Kukla C, Felfer P (2019) Fused filament fabrication, debinding and sintering as a low cost additive manufacturing method of 316L stainless steel. Addit Manuf 30:100861. https://doi.org/10.1016/j.addma.2019.100861
24. Wagner MA, Engel J, Hadian A, Clemens F, Rodriguez-Arbaizar M, Carreño-Morelli E, Wheeler JM, Spolenak R (2022) Filament extrusion-based additive manufacturing of 316L stainless steel: effects of sintering conditions on the microstructure and mechanical properties. Addit Manuf 59:103147. https://doi.org/10.1016/j.addma.2022.103147
25. Quarto M, Carminati M, D'Urso G (2021) Density and shrinkage evaluation of AISI 316L parts printed via FDM process. Mater Manuf Proces 36:1535–1543. https://doi.org/10.1080/10426914.2021.1905830
26. Obadimu SO, Kourousis KI (2022) Shrinkage behaviour of material extrusion steel 316L: influence of primary 3D printing parameters. RPJ 28:92–101. https://doi.org/10.1108/RPJ-07-2022-0224
27. Gong H, Snelling D, Kardel K, Carrano A (2019) Comparison of stainless steel 316L parts made by FDM- and SLM-based additive manufacturing processes. JOM 71:880–885. https://doi.org/10.1007/s11837-018-3207-3
28. Hassan W, Farid MA, Tosi A, Rane K, Strano M (2021) The effect of printing parameters on sintered properties of extrusion-based additively manufactured stainless steel 316L parts. Int J Adv Manuf Technol 114:3057–3067. https://doi.org/10.1007/s00170-021-07047-w
29. Tosto C, Tirillò J, Sarasini F, Cicala G (2021) Hybrid metal/polymer filaments for fused filament fabrication (FFF) to print metal parts. Appl Sci 11:1444. https://doi.org/10.3390/app11041444
30. Butt J, Bhaskar R, Mohaghegh V (2022) Investigating the effects of ironing parameters on the dimensional accuracy, surface roughness, and hardness of FFF-printed thermoplastics. J Compos Sci 6:121. https://doi.org/10.3390/jcs6050121
31. Sardinha M, Lopes J, Gusmão A, Reis L, Leite M (2022) Ironing process influence on the warping of ABS parts produced by fused filament fabrication. Procedia Struct Integrity 42:1274–1281. https://doi.org/10.1016/j.prostr.2022.12.162
32. Sardinha M, Vicente CMS, Frutuoso N, Leite M, Ribeiro R, Reis L (2021) Effect of the ironing process on ABS parts produced by FDM. Mat Design Process Comms 3. https://doi.org/10.1002/mdp2.151
33. Caputo M, Rashwan O, Waryoba D, McDade K (2022) Surface texture and thermo-mechanical properties of material extruded and ironed polylactic acid. Addit Manuf 59:103084. https://doi.org/10.1016/j.addma.2022.103084
34. Alzyod H, Ficzere P (2024) Ironing process optimization for enhanced properties in material extrusion technology using Box-Behnken design. Sci Rep 14:2300. https://doi.org/10.1038/s41598-024-52827-5
35. Neuhaus B, Idris MK, Naderi P, El-Hajj Y, Grau G (2024) Low-roughness 3D-printed surfaces by ironing for the integration with printed electronics. Adv Eng Mater 26:2301711. https://doi.org/10.1002/adem.202301711
36. The Virtual Foundry Stainless Steel 316L technical data sheet. Available online: https://thevirtualfoundry.com/wp-content/uploads/2024/04/The-Virtual-Foundry-TDS-Stainless-Steel-316L-24-04.pdf. Accessed on 02 May 2024
37. The Virtual Foundry Stainless Steel 316L safety data sheet. Available online: https://thevirtualfoundry.com/wp-content/uploads/2024/03/The-Virtual-Foundry-SDS-Stainless-Steel-316L-24-01.pdf. Accessed on 02 May 2024
38. Rosnitschek T, Hueter F, Alber-Laukant B (2020) FEM-based modelling of elastic properties and anisotropic sinter shrinkage of metal EAM. Int j simul model 19:197–208. https://doi.org/10.2507/IJSIMM19-2-509